

Facile Synthesis and Characterization of $\text{Li}_4\text{Ti}_5\text{O}_{12}$ as Anode Material for Lithium Ion Batteries

Ling-Ling Xie, Yuan-Dong Xu, Jie-Jie Zhang, Xiao-Yu Cao*, Bo Wang, Xiang-Yang Yan, Ling-Bo Qu

School of Chemistry and Chemical Engineering, Henan University of Technology, Zhengzhou 450001, People's Republic of China

*E-mail: caoxy@haut.edu.cn

Received: 9 December 2012 / Accepted: 6 January 2013 / Published: 1 February 2013

$\text{Li}_4\text{Ti}_5\text{O}_{12}$ was successfully synthesized through the liquid phase evaporation reaction using lithium hydroxide ($\text{LiOH}\cdot\text{H}_2\text{O}$) and butyl titanate ($\text{C}_{16}\text{H}_{36}\text{O}_4\text{Ti}$) as raw materials. The as-prepared powders were characterized by means of powder X-ray diffraction (XRD) and scanning electron microscope (SEM), and the electrochemical properties of the $\text{Li}_4\text{Ti}_5\text{O}_{12}$ powders were examined by the galvanostatic charge/discharge and cyclic voltammetry (CV) tests. The results indicate that the sintering temperature has a remarkable effect on the structure, morphology, and electrochemical performances. $\text{Li}_4\text{Ti}_5\text{O}_{12}$ powder synthesized at 650 °C for 20 h displays well-developed crystal structure and well-crystallized micro-sized particles. The apparent diffusion coefficients of Li^+ ions calculated from CV are in the order of 10^{-7} – 10^{-6} $\text{cm}^2 \text{s}^{-1}$. Electrochemical analyses show that 650 °C-synthesized $\text{Li}_4\text{Ti}_5\text{O}_{12}$ powder exhibits good cycling performance of 146.63 mAh g^{-1} after 100 cycles at the current of 30 mA g^{-1} and a superior rate capability of 125.77 mAh g^{-1} at the current of 120 mA g^{-1} .

Keywords: Liquid phase evaporation reaction; Characterization; $\text{Li}_4\text{Ti}_5\text{O}_{12}$; Anode material; Rate capability; Lithium ion batteries

1. INTRODUCTION

Of all the commercialized rechargeable batteries, lithium ion batteries (LIBs) have widely used in portable electronic devices such as cellphone, camcorder, MP4, PDA, and laptop due to large energy density, high output voltage, and long cycling life. Meanwhile, it is highly anticipated that LIBs could be universally used in hybrid electric vehicles (HEVs) and electric vehicles (EVs) [1,2] in the future. However, the security concerns of LIBs must be addressed if HEVs and EVs powered by LIBs want to achieve a large-scale application in spite of the present situation that HEVs and EVs have been in running in dribs and drabs in some cities. The safety hazards mainly originate from the approximative

lithium intercalation potentials of graphite and metal lithium [3], which easily leads to the growth of lithium dendrite on anode surface and consequently incites short circuit and explosion at high rate charge/discharge regime. In order to overcome this problem, one of effective ways is to adopt an electrochemical redox couple with higher equilibrium potentials, thus resulting in the formation of lithium dendrite thermodynamically less favorable.

Spinel $\text{Li}_4\text{Ti}_5\text{O}_{12}$ displays a flat voltage plateau located around 1.55 V vs. Li/Li^+ , which is higher than the conventional carbonous materials and fulfills this requirement. The low formation enthalpy ($-6061.45 \pm 4 \text{ kJ mol}^{-1}$) indicates that spinel $\text{Li}_4\text{Ti}_5\text{O}_{12}$ has a high thermodynamic stability [4]. In addition, both the excellent Li^+ intercalation/deintercalation kinetics and structural stability make it achieve the high rate capability and reversibility, which is known as zero-strain insertion material. Furthermore, $\text{Li}_4\text{Ti}_5\text{O}_{12}$ is cheap and non-toxic compared to other anode materials, and production of $\text{Li}_4\text{Ti}_5\text{O}_{12}$ anode material conforms to the idea of constructing environment-friendly society. Therefore, the aforementioned advantages of $\text{Li}_4\text{Ti}_5\text{O}_{12}$ have stirred up a continuous interest for many researchers though the energy density of LIBs is slightly sacrificed when it is coupled with a 4 V cathode material [5].

However, the preparation methods are very critical to the exhibition of excellent electrochemical performances for $\text{Li}_4\text{Ti}_5\text{O}_{12}$ anode material [3] because they control the structure, morphology, particle size, and particle size distribution amongst other critical parameters. In the case of preparation methods, $\text{Li}_4\text{Ti}_5\text{O}_{12}$ has been widely prepared by various synthetic methods [3,6]. Of these synthetic methods, the conventional solid state synthesis methods (CSSYMs) are usually used to synthesize $\text{Li}_4\text{Ti}_5\text{O}_{12}$ powder at high temperature starting from lithium salts and titanium oxides [7–15]. But some CSSYMs are energy intensive and cannot readily produce peculiarly electrochemical performances. At the same time, CSSYMs-derived $\text{Li}_4\text{Ti}_5\text{O}_{12}$ powders often encounter low homogeneity, irregular morphology, and undesirable large particle size owing to the high calcinations temperature and prolonged calcination time, thus incurring an adverse effect on its electrochemical performances such as discharge capacity and rate capability. Especially, some CSSYMs need to be performed in a nitrogen or oxygen gas stream [7–10,12], which leads to the cost increase. The soft chemistry synthesis methods (SCSMs) for $\text{Li}_4\text{Ti}_5\text{O}_{12}$ powders such as the sol–gel synthesis method [16,17], the combustion synthesis method [18,19], the spray drying method [20,21], the macroemulsion and microemulsion synthesis method [22,23], the hydrothermal synthesis method [24,25], the reverse micelle method [26], the electrospinning synthesis method [27], the microwave synthesis method [28] have been made under more milder condition. Due to mixing the raw materials at the atomic scale or preparing the precursors composed of ultra-fine particles, the particle size of SCSMs-derived $\text{Li}_4\text{Ti}_5\text{O}_{12}$ powders with various morphologies is much finer and more uniform compared to the CSSYMs-derived $\text{Li}_4\text{Ti}_5\text{O}_{12}$ powders. As a result, SCSMs-derived $\text{Li}_4\text{Ti}_5\text{O}_{12}$ powders obtained at lower temperature display the high discharge capacity and excellent rate capability.

Here, we introduce a facile synthesis process for preparing the micro-sized $\text{Li}_4\text{Ti}_5\text{O}_{12}$ powders by liquid phase evaporation (LPE) method. The structure, morphology, and electrochemical performances of the as-synthesized $\text{Li}_4\text{Ti}_5\text{O}_{12}$ powders, including cycling stability and rate capability, were extensively investigated.

2. EXPERIMENTAL

The raw materials used in this work were lithium hydroxide ($\text{LiOH}\cdot\text{H}_2\text{O}$) and butyl titanate ($\text{C}_{16}\text{H}_{36}\text{O}_4\text{Ti}$), being all of analytical grade and as received. $\text{Li}_4\text{Ti}_5\text{O}_{12}$ powders were prepared through a facile wet chemical synthesis method, namely, LPE method as described in our previous reports [29–31]. Stoichiometric ratios of $\text{LiOH}\cdot\text{H}_2\text{O}$ and $\text{C}_{16}\text{H}_{36}\text{O}_4\text{Ti}$ were mixed in a beaker under magnetic stirring electric heater, followed by adding redistilled water dropwise. When hydrolysis of $\text{C}_{16}\text{H}_{36}\text{O}_4\text{Ti}$ was stopped, then the liquid phase mixture was evaporated in a bath at $80\text{ }^\circ\text{C}$ for 5 h until the slurry residue was obtained. Afterwards, the slurry was allowed to dry at $100\text{ }^\circ\text{C}$ followed by grinding, which yields a material, referred to as the $\text{Li}_4\text{Ti}_5\text{O}_{12}$ precursor. Finally, $\text{Li}_4\text{Ti}_5\text{O}_{12}$ powders were obtained by sintering precursor in a muffle furnace (CMF-1100X, Zhengzhou Kejing Thermal Technology Co., Ltd) in the range of $600\text{ }^\circ\text{C}$ – $750\text{ }^\circ\text{C}$ for 20 h and then cooling to room temperature.

X-ray diffraction (XRD) analysis was carried out on an XRD-6000 diffractometer (Shimadzu) with $\text{Cu K}\alpha$ radiation ($\lambda = 1.54056\text{ \AA}$). The morphological feature of the thus-prepared powders was observed on the SEM-JSM-6510LV (JEOL, Japan). The working electrodes were composed of $\text{Li}_4\text{Ti}_5\text{O}_{12}$ powders, acetylene black and polytetrafluoroethylene emulsion binder (60 wt. %, Xinxiang Yilida Batteries Materials Co., Ltd) at a weight ratio of 80:10:10. The stainless-steel meshes were used as the current collectors. The CR2016 coin cells were assembled with pure lithium foil as a counter electrode, Celgard-2400 as the separator and 1 mol dm^{-3} LiClO_4 dissolved in ethylene carbonate (EC) and dimethyl carbonate (DMC) solution (v/v of 1:1, provided by Zhangjiagang Guotai-Huarong New Chemical Materials Co., Ltd) as the electrolyte. All the CR2016 type coin cells were assembled in a high purified argon-filled dry box (JMS-3, Nanjing Jiumen Automation technology Co., Ltd). Galvanostatic charge/discharge cycle tests were performed on a on a multi-channel CT-3008W-5V5mA-S₄ battery system (Shenzhen Neware Electronics Co., Ltd) at ambient temperature with different current densities in the potential range of 1.0–3.0 V vs. Li^+/Li . Cyclic voltammetry (CV) studies were carried out on a CHI660D electrochemical workstation (Shanghai Chenhua Crop) at different scan rates by using lithium foils as the reference and the counter electrodes.

3. RESULTS AND DISCUSSION

The XRD patterns of LPE-derived $\text{Li}_4\text{Ti}_5\text{O}_{12}$ powders heat-treated at $600\text{ }^\circ\text{C}$ – $750\text{ }^\circ\text{C}$ for 20 h are shown in Fig. 1. According to XRD patterns, the intensities of Bragg diffraction peaks of as-synthesized $\text{Li}_4\text{Ti}_5\text{O}_{12}$ powders are heightened with increasing of sintering temperature. In the case of powder heated at $600\text{ }^\circ\text{C}$ for 20 h in Fig. 1(a), the main Bragg diffraction peaks of $\text{Li}_4\text{Ti}_5\text{O}_{12}$ phase have emerged other than impurity peaks marked with snowflake-like symbol (*) which are ascribed to anatase TiO_2 . With increasing of the sintering temperatures, impurity peaks gradually disappear. From $700\text{ }^\circ\text{C}$, all the peaks of as-prepared powders exhibit the characteristic diffraction lines of $\text{Li}_4\text{Ti}_5\text{O}_{12}$ phase without presence of any detectable impurity, which can be identified as $[\text{Li}]_{8a}[\text{Li}_{1/3}\text{Ti}_{5/3}]_{16d}[\text{O}_{12}]_{32e}$ and indexed to the cubic system with space group $Fd\bar{3}m$. These phenomena

indicate that sintering temperature plays an important role in facilitating a well-developed crystal structure.

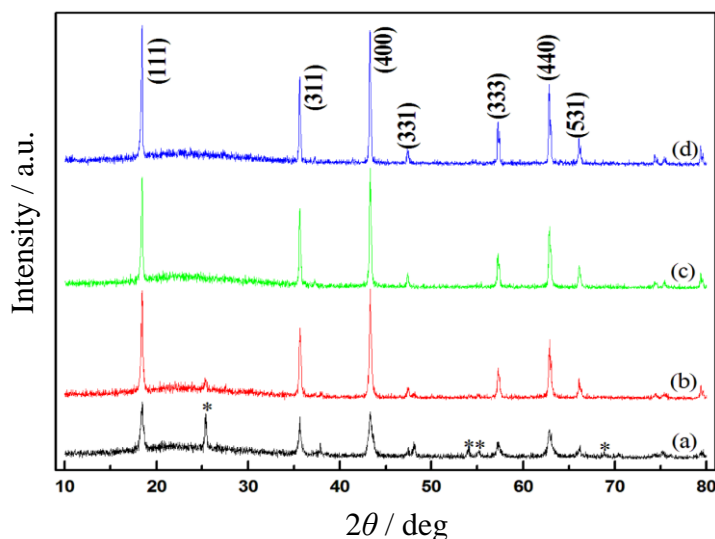


Figure 1. XRD patterns of $\text{Li}_4\text{Ti}_5\text{O}_{12}$ powders calcined at different temperatures for 20 h (a) 600 °C, (b) 650 °C, (c) 700 °C, and (d) 750 °C.

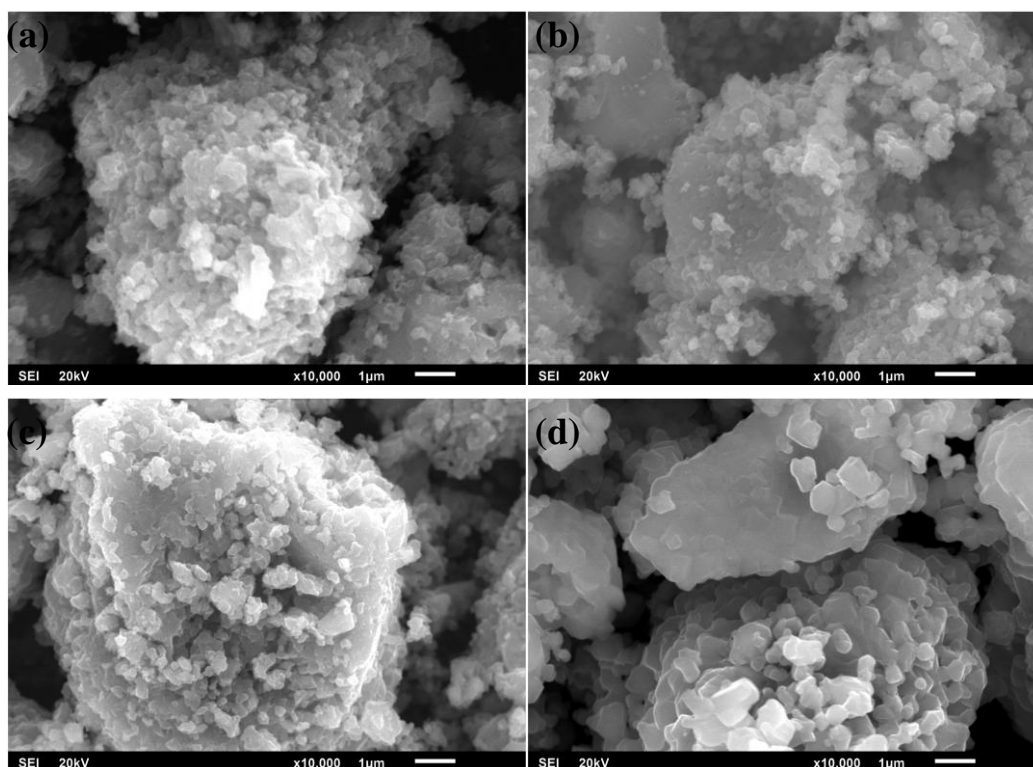


Figure 2. SEM images of $\text{Li}_4\text{Ti}_5\text{O}_{12}$ powders calcined at different temperatures for 20 h (a) 600 °C, (b) 650 °C, (c) 700 °C, and (d) 750 °C.

Fig. 2 show SEM images of LPE-derived $\text{Li}_4\text{Ti}_5\text{O}_{12}$ powders obtained at different temperatures for 20 h. It is obvious that sintering temperature causes some changes in morphology. In the case of the $\text{Li}_4\text{Ti}_5\text{O}_{12}$ powder calcined at 600 °C for 20 h in Fig. 2(a), large secondary particles with severe agglomeration are found to be composed of small primary grains. With sintering temperature increasing, 650 °C– and 700 °C–synthesized $\text{Li}_4\text{Ti}_5\text{O}_{12}$ powders fractionate out and evolve into some smaller and somewhat fluffy grains. When the sintering temperature is increased to 750 °C, the powder displays a mixture of some large plate-like particles and the rest agglomerated particles, hinting that morphological evolution of agglomerated grains into plate-like shape. On the whole, 650 °C–synthesized $\text{Li}_4\text{Ti}_5\text{O}_{12}$ powder exhibits a smaller particle size and well developed crystalline compared to other $\text{Li}_4\text{Ti}_5\text{O}_{12}$ powders. It is generally acknowledged that insertion of Li^+ ions in bulk material is a diffusion process. Thus, smaller grains will lead to shorter transport length for both electrons and Li^+ ions [32], which are beneficial for $\text{Li}_4\text{Ti}_5\text{O}_{12}$ anode material to both reversible capacity and cyclability. As a result, a better electrochemical performance for the $\text{Li}_4\text{Ti}_5\text{O}_{12}$ powder calcined at 650 °C for 20 h is to follow on.

Fig. 3 shows the initial discharge/charge voltage profiles of $\text{Li}_4\text{Ti}_5\text{O}_{12}$ powders at the current density of 30 mA g^{-1} in the voltage range of 1.0–3.0 V. As shown in Fig. 3, 600 °C–synthesized $\text{Li}_4\text{Ti}_5\text{O}_{12}$ powder manifests a smooth discharge curve with a discharge capacity of 153.07 mAh g^{-1} . The discharge platform around 1.52 V is a characteristic of the mutual transformation of $\text{Ti}^{4+}/\text{Ti}^{3+}$ redox couple. However, charge curve of 600 °C–synthesized $\text{Li}_4\text{Ti}_5\text{O}_{12}$ powder exhibits a repeated elevating trend, which obviously originates from its undeveloped crystal structure due to the existence of anatase TiO_2 impurity in XRD patterns. For the $\text{Li}_4\text{Ti}_5\text{O}_{12}$ powder synthesized at 650 °C, it almost displays smooth discharge/charge curves though small amounts of impurities can be detected in XRD patterns. Moreover, initial discharge/charge capacities of 650 °C–synthesized $\text{Li}_4\text{Ti}_5\text{O}_{12}$ powder amount to 177.15/163.01 mAh g^{-1} , which is the highest among all the synthesized $\text{Li}_4\text{Ti}_5\text{O}_{12}$ anodes. As aforementioned, smaller particles can result in shorter transport length for both electrons and Li^+ ions, which can reduce the concentration polarization and certainly contribute to high discharge/charge capacities for the resultant $\text{Li}_4\text{Ti}_5\text{O}_{12}$ powder heated at 650 °C. Additionally, according to the recent reports [33,34], the appropriate amount of residual anatase TiO_2 in $\text{Li}_4\text{Ti}_5\text{O}_{12}$ phase is beneficial to improving the electrochemical performances of $\text{Li}_4\text{Ti}_5\text{O}_{12}$, which may be also an important factor for 650 °C–synthesized $\text{Li}_4\text{Ti}_5\text{O}_{12}$ powder to be displayed the highest discharge/charge capacities. With increase of particle size, the $\text{Li}_4\text{Ti}_5\text{O}_{12}$ powder heated at 700 °C demonstrates a low discharge/charge capacities (152.7/161 mAh g^{-1}) compared to the $\text{Li}_4\text{Ti}_5\text{O}_{12}$ powder heated at 650 °C because of its prolonged diffusion path for Li^+ ions. As for the $\text{Li}_4\text{Ti}_5\text{O}_{12}$ powder heated at 750 °C, its discharge/charge plateaus are substantially shortened, thus leading to a lowest discharge/charge capacity (150.44/140.19 mAh g^{-1}).

Fig. 4 shows the cycle performance of all gained $\text{Li}_4\text{Ti}_5\text{O}_{12}$ powders at the current density of 30 mA g^{-1} . It can be seen that the 650 °C–synthesized $\text{Li}_4\text{Ti}_5\text{O}_{12}$ powder delivers an initial discharge capacity of 177.15 mAh g^{-1} and remains 146.63 mAh g^{-1} at the end of 100th cycle. Meanwhile, the 700 °C–synthesized $\text{Li}_4\text{Ti}_5\text{O}_{12}$ powder also behaves a better cycleability with a capacity of 142.74 mAh g^{-1} after 100 cycles. In contrast, 600 °C– and 750–synthesized $\text{Li}_4\text{Ti}_5\text{O}_{12}$ powders exhibits a lower

capacity and worse cycleability. The results indicate that the sintering temperature has a remarkable effect on the capacity and cyclic behavior.

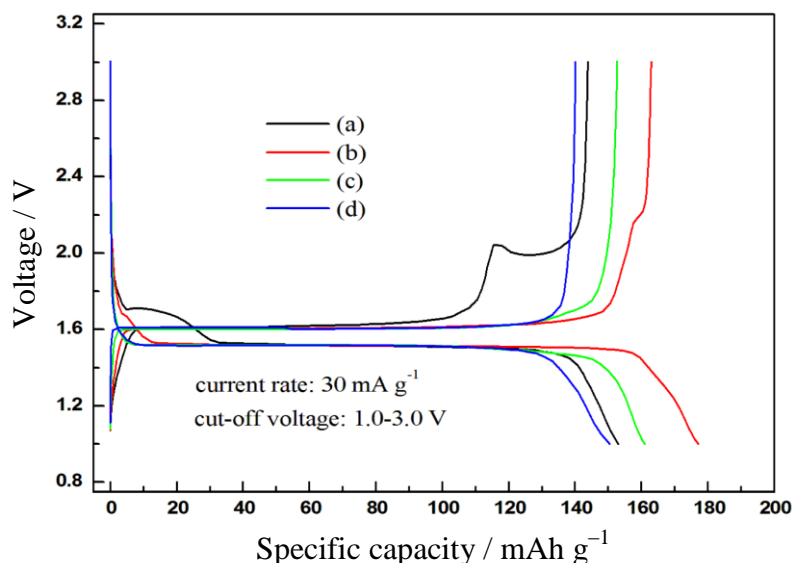


Figure 3. The initial discharge/charge curves of $\text{Li}_4\text{Ti}_5\text{O}_{12}$ powders obtained at different temperatures for 20 h (a) 600 °C, (b) 650 °C, (c) 700 °C, and (d) 750 °C.

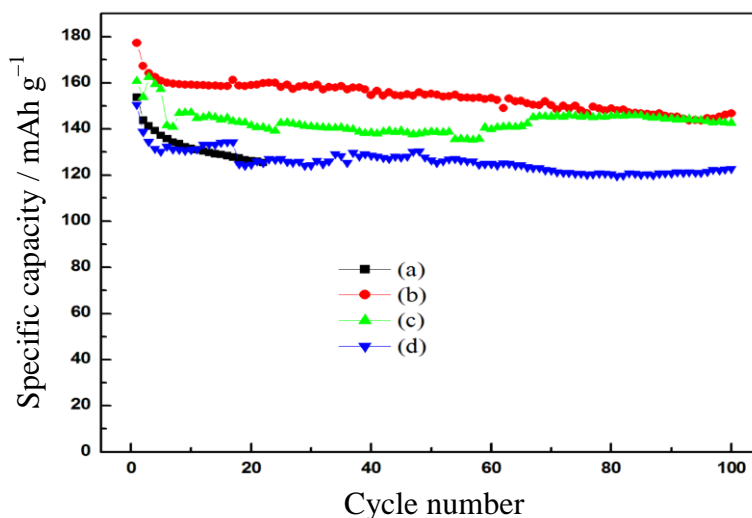


Figure 4. Variation of discharge capacity vs. cycle number using the as-synthesized $\text{Li}_4\text{Ti}_5\text{O}_{12}$ powders as electrodes (a) 600 °C, (b) 650 °C, (c) 700 °C, and (d) 750 °C.

The initial discharge/charge curves of $\text{Li}_4\text{Ti}_5\text{O}_{12}$ powder obtained at 650 °C for 20 h at the current rates of 30 mA g^{-1} –120 mA g^{-1} are presented in Fig. 5. As shown in Fig. 5, 650 °C–synthesized $\text{Li}_4\text{Ti}_5\text{O}_{12}$ powder yields the initial discharge/charge capacities of 177.15/163.01 mAh g^{-1} , 167.17/162.64 mAh g^{-1} , 156/147.44 mAh g^{-1} , and 147.15/143.06 mAh g^{-1} at the current rates of 30

mA g^{-1} , 60 mA g^{-1} , 90 mA g^{-1} , and 120 mA g^{-1} , respectively. With intensifying of electrode polarization, discharge plateau of as-prepared $\text{Li}_4\text{Ti}_5\text{O}_{12}$ powder begins to decline, while discharge plateaus are nearly at constant potential ca. around 1.33 V starting from the current rate of 60 mA g^{-1} . The results indicate the superiority of $650 \text{ }^\circ\text{C}$ -synthesized $\text{Li}_4\text{Ti}_5\text{O}_{12}$ powder as high rate anode material for Li ion batteries.

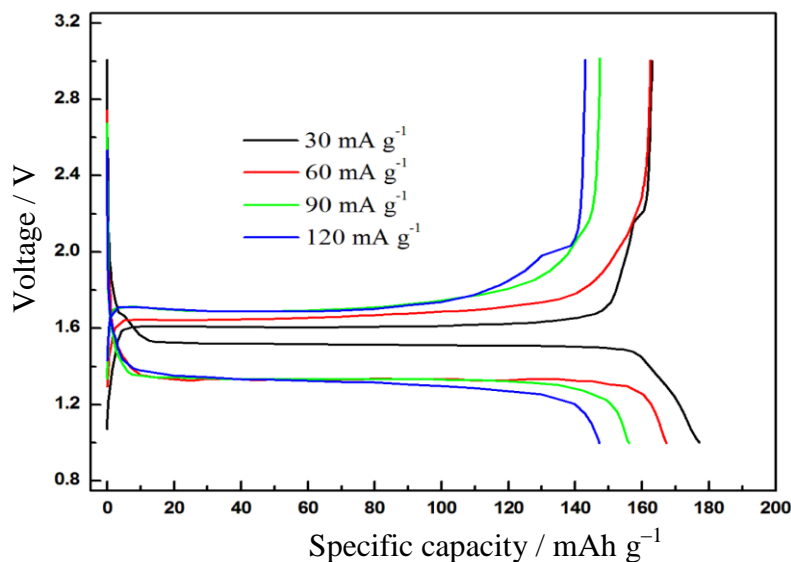


Figure 5. The initial discharge/charge curves of $\text{Li}_4\text{Ti}_5\text{O}_{12}$ powder obtained at $650 \text{ }^\circ\text{C}$ for 20 h at the different current rates.

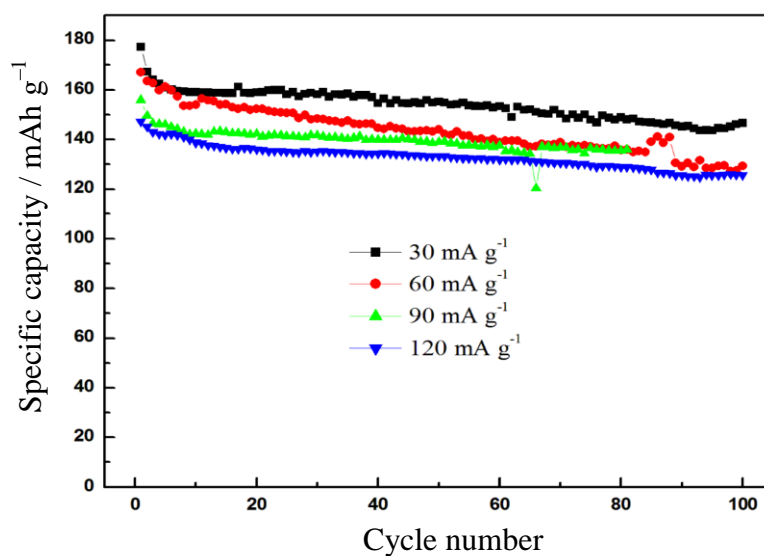


Figure 6. Cycling stability of as-synthesized $\text{Li}_4\text{Ti}_5\text{O}_{12}$ powders at $650 \text{ }^\circ\text{C}$ for 20 h at different current rates.

Fig. 6 gives cycling stability of as-synthesized $\text{Li}_4\text{Ti}_5\text{O}_{12}$ powders at $650\text{ }^\circ\text{C}$ for 20 h at current rates of 30 mA g^{-1} – 120 mA g^{-1} . It is found that $650\text{ }^\circ\text{C}$ –synthesized $\text{Li}_4\text{Ti}_5\text{O}_{12}$ powder displays excellent cyclic performance in all cases even if operated at 120 mA g^{-1} for 100 cycles, which implies that an excellent rate capability can be achieved without carbon coating. Generally, carbon coating or ionic doping is essential for preparing $\text{Li}_4\text{Ti}_5\text{O}_{12}$ powders with high rate performance [3]. However, neither carbon coating nor ionic doping is used for modifying $\text{Li}_4\text{Ti}_5\text{O}_{12}$ in the LPE processes, indicating the superiority of LPE method in this work. The better performance of $650\text{ }^\circ\text{C}$ –synthesized $\text{Li}_4\text{Ti}_5\text{O}_{12}$ powder may be ascribed to the following three aspects: first, in comparison with $600\text{ }^\circ\text{C}$ –synthesized $\text{Li}_4\text{Ti}_5\text{O}_{12}$ powder, $650\text{ }^\circ\text{C}$ –synthesized $\text{Li}_4\text{Ti}_5\text{O}_{12}$ powder has less impurities and well-developed crystal structure. Second, residual anatase TiO_2 in $\text{Li}_4\text{Ti}_5\text{O}_{12}$ phase is in favor of exhibiting good rate capability over individual single-phase $\text{Li}_4\text{Ti}_5\text{O}_{12}$ [34]. Third, particle size of $650\text{ }^\circ\text{C}$ –synthesized $\text{Li}_4\text{Ti}_5\text{O}_{12}$ powder is smaller than those of other $\text{Li}_4\text{Ti}_5\text{O}_{12}$ powders, which can shorten transport length for both electrons and Li^+ ions in bulk material.

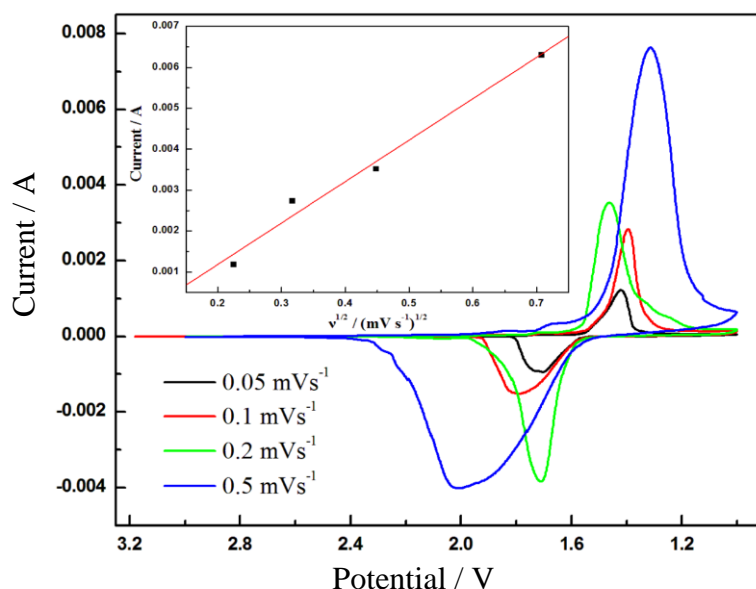


Figure 7. CV of as-synthesized $\text{Li}_4\text{Ti}_5\text{O}_{12}$ powder at $650\text{ }^\circ\text{C}$ for 20 h at different sweep rates.

Fig. 7 shows the initial CV measured at different scanning rates from 0.05 mV s^{-1} to 0.5 mV s^{-1} between 1.0 and 3.0 V. At the scan rate of 0.05 mV s^{-1} , there is one pair of redox peaks, which should be attributed to the redox of $\text{Ti}^{4+}/\text{Ti}^{3+}$ couple. The well-defined cathode and anode peak centered at 1.422 V and 1.702 V indicates a high crystallinity, as reflected in XRD patterns. When the scanning rate is increased, the shape of the cathodic and anodic peaks becomes unsymmetrical, indicating an increased electrode polarization. At the same time, the heights of cathodic and anodic peaks increase with the increase in potential sweep rate. The inset in Fig.7 is an expanded view of the relation of the reduction peak currents and the square roots of the scanning rates. It is clearly seen that the reduction

peak currents have a good linear relationship with the square roots of the scanning rates in the scanning rates range of 0.05–0.5 mV s^{-1} , indicating that the redox process of $\text{Li}_4\text{Ti}_5\text{O}_{12}$ powder is a diffusion-limited intercalation processes of Li^+ ions [35]. It is not difficult to understand that the rapid transport of Li^+ ions from the bulk electrolyte solution to the surface of $\text{Li}_4\text{Ti}_5\text{O}_{12}$ powder will not maintain when the discharge/charge current significantly increases, and Li^+ ions diffusion accordingly becomes control step for the overall electrochemical reaction.

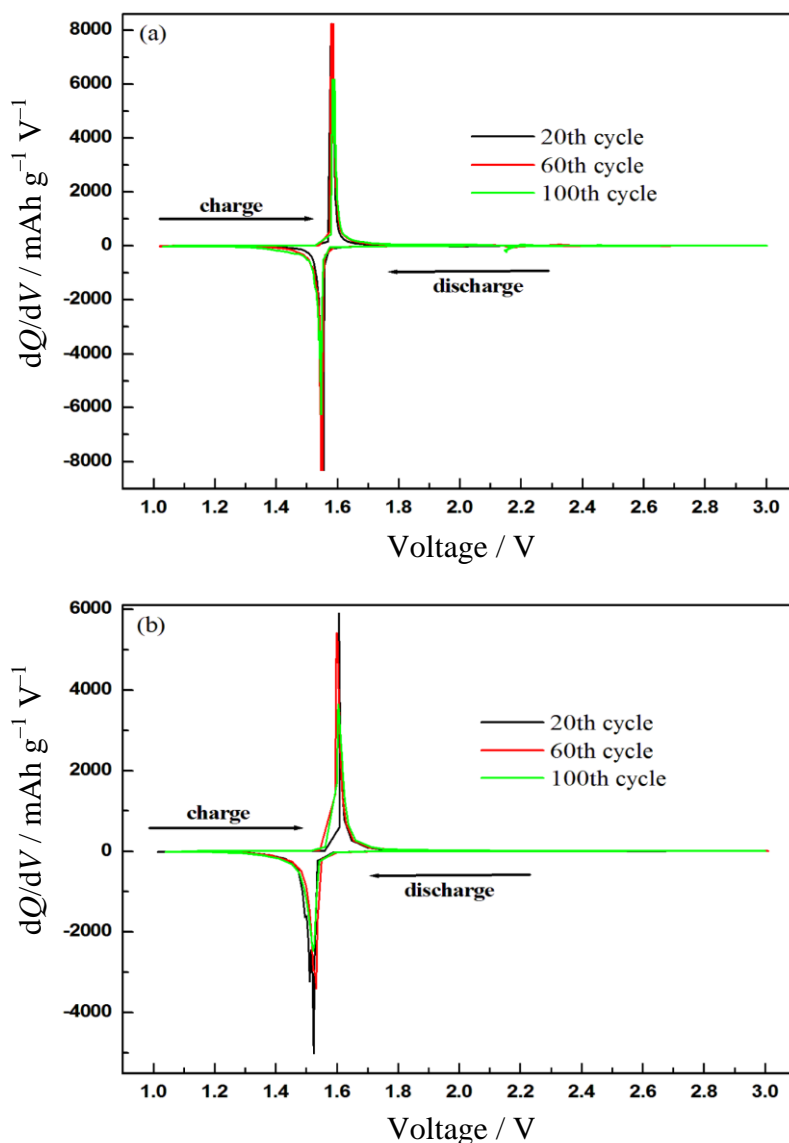


Figure 8. Different capacity vs voltage curves of as-synthesized $\text{Li}_4\text{Ti}_5\text{O}_{12}$ powder at $650\text{ }^\circ\text{C}$ for 20 h at the different current rates. (a) 30 mA g^{-1} , and (b) 120 mA g^{-1} .

According to Randles–Sevchik equation: $I_p = 0.4463n^{3/2}FAf^{1/2}D^{1/2}v^{1/2}C_{\text{Li}^+}$ [36], the apparent diffusion coefficient of Li^+ in $\text{Li}_4\text{Ti}_5\text{O}_{12}$ powder can be calculated, where I_p is the peak current (amperes), n the charge-transfer number, A the surface area in cm^2 of the electrode, D the chemical

diffusion coefficient ($\text{cm}^2 \text{s}^{-1}$), ν the scanning rate (V s^{-1}), C_{Li^+} the bulk concentration of Li^+ ions in electrode (mol cm^{-3}), and $f = F/RT$ where F is Faraday constant, R the gas constant and T the absolute temperature. Based on Randles–Sevchik equation, the apparent diffusion coefficient of Li^+ ions could be calculated to be $6.47 \times 10^{-7} \text{ cm}^2 \text{ s}^{-1}$, $1.7 \times 10^{-6} \text{ cm}^2 \text{ s}^{-1}$, $1.4 \times 10^{-6} \text{ cm}^2 \text{ s}^{-1}$, and $1.79 \times 10^{-6} \text{ cm}^2 \text{ s}^{-1}$ at the scanning rates of 0.05 mV s^{-1} , 0.1 mV s^{-1} , 0.2 mV s^{-1} , and 0.5 mV s^{-1} , respectively. The calculated results disclose that the apparent diffusion coefficient of Li^+ ions is in the range of $10^{-7} \text{ cm}^2 \text{ s}^{-1}$ to $10^{-6} \text{ cm}^2 \text{ s}^{-1}$, which is higher than the reported value [37] and in good agreement with rate capability reflected in Fig.6.

In order to emphasize the details of the discharge/charge voltage profiles, the plots of differential capacity vs voltage (dQ/dV vs V) at the current rates of 30 mA g^{-1} and 120 mA g^{-1} at the 20th, 60th, and 100th cycle are illustrated in Fig. 8. The sharp peaks on the dQ/dV vs V plots mean that insertion/deinsertion of Li^+ ions proceeds through a few multiphase regions until the limit of reversible lithium uptake is reached. In the case of the dQ/dV vs V curves at the current rate of 30 mA g^{-1} , one reduction peak around 1.55 V and one oxidation peak around 1.58 V can be observed, and small the potential difference (ΔE , e.g. 0.03 V) of the redox of $\text{Ti}^{4+}/\text{Ti}^{3+}$ couple indicates an excellent reversibility of Li^+ intercalation into and deintercalation from $\text{Li}_4\text{Ti}_5\text{O}_{12}$ powder. Beside this, the dQ/dV vs V curves are almost coincident with each other at the 20th, 60th, and 100th cycle, which suggests that LPE-derived $\text{Li}_4\text{Ti}_5\text{O}_{12}$ powder treated at $650 \text{ }^\circ\text{C}$ exhibits a superior structural stability. With increasing the current rates from 30 mA g^{-1} to 120 mA g^{-1} , ΔE (e.g. 0.083 V) is still minor though it trends to become slightly larger in comparison with the dQ/dV vs V curves at the current rate of 30 mA g^{-1} . Meanwhile, the dQ/dV vs V curves at the current rate of 120 mA g^{-1} are also well overlapped.

Based on the above-mentioned results, the conclusion can be reached that the $\text{Li}_4\text{Ti}_5\text{O}_{12}$ powder synthesized at $650 \text{ }^\circ\text{C}$ by the wet chemistry synthetic route of this work displays the excellent cycleability and rate capability and can be employed as a long-lived and high power anode material for lithium ion batteries.

4. CONCLUSIONS

LPE reaction derived $\text{Li}_4\text{Ti}_5\text{O}_{12}$ powders have been successfully synthesized in this work. The calcinations temperature has an important effect on the structure and electrochemical behaviors. The as-synthesized $\text{Li}_4\text{Ti}_5\text{O}_{12}$ powders display high crystallinity and well-developed crystal structure from $650 \text{ }^\circ\text{C}$. SEM results show that well-crystallized $\text{Li}_4\text{Ti}_5\text{O}_{12}$ powder with small particles is obtained at $650 \text{ }^\circ\text{C}$ for 20 h. The $\text{Li}_4\text{Ti}_5\text{O}_{12}$ powder made at $650 \text{ }^\circ\text{C}$ for 20 h yields the first discharge capacity of as high as $177.15 \text{ mAh g}^{-1}$ with a voltage range of $1.0\text{--}3.0 \text{ V}$ at the current rate of 30 mA g^{-1} and remains $146.63 \text{ mAh g}^{-1}$ after 100 cycles. Even if operated at 120 mA g^{-1} for 100 cycles, the discharge capacity of $125.77 \text{ mAh g}^{-1}$ is still maintained, indicating that a high rate capability may arise from the high apparent diffusion coefficients of Li^+ ions ($6.47 \times 10^{-7} \text{ cm}^2 \text{ s}^{-1}$ – $1.79 \times 10^{-6} \text{ cm}^2 \text{ s}^{-1}$). This also means that the appropriate amount of residual anatase TiO_2 in $\text{Li}_4\text{Ti}_5\text{O}_{12}$ phase is beneficial to improving the electrochemical performances. In sum, this LEP process demonstrates to be an effective and promising

method for synthesizing a long-lived and high power anode material $\text{Li}_4\text{Ti}_5\text{O}_{12}$ for lithium ion batteries.

ACKNOWLEDGMENTS

This work was supported by Program for Science & Technology Innovation Talents in Universities of Henan Province (HASTIT), China (Grant No. 2011HASTIT017), Young Core Teacher Program in Higher Education Institutions from the Education Commission of Henan Province, China (Grant No. 2009GGJS-059), Key Science and Technology Project of Henan Province, China (Grant Nos. 092102210153,122102210114), Basic Science and Technological Frontier Project of Henan Province, China (Grant No. 092300410117), and Zhengzhou Municipal Science & Technology Development Programs, China (Grant Nos. 112PZDZX019, 20110285).

References

1. P.G. Bruce, B. Scrosati, J. M. Tarascon, *Angew. Chem. Int. Ed.* 47 (2008) 2930.
2. J.W. Fergus, *J. Power Sources* 195 (2010) 939.
3. T.F. Yi, L.J. Jiang, J. Shu, C.B. Yue, R.S. Zhu, H.B. Qiao, *J. Phys. Chem. Sol.* 71 (2010) 1236.
4. T.F. Yi, Y. Xie, Y.R. Zhu, R.S. Zhu, H.Y. Shen, *J. Power Sources* 222 (2013) 448.
5. L.L. Xie, X.Y. Cao, C.W. Liu, C.W. Wang, *J. Chil. Chem. Soc.* 55 (2010) 343.
6. G.N. Zhu, Y.G. Wang, Y.Y. Xia, *Energy Environ. Sci.* 5 (2012) 6652.
7. T. Ohzuku, A. Ueda, N. Yamamoto, *J. Electrochem. Soc.* 142 (1995)1431.
8. K. Zaghib, M. Armand, M. Gauthier, *J. Electrochem. Soc.*145 (1999) 3135.
9. K. Zaghib, M. Simoneau, M. Armand, M. Gauthier, *J. Power Sources* 81–82 (1999) 300.
10. S. Scharner, W. Weppner, P. Schmid-Beurmann, *J. Electrochem. Soc.*146 (1999) 857.
11. G.X. Wang, D.H. Bradhurst, S.X. Dou, H.K. Liu, *J. Power. Sources* 83 (1999) 156.
12. S. Panero, P. Reale, F. Ronci, V. Rossi Albertini, B. Scrosati, *Ionics* 6 (2000) 461.
13. F.X. Wu, Z.X. Wang, X.H. Li, L. Wu, X.J. Wang, X.P. Zhang, Z.G. Wang, X.H. Xiong, H.J. Gu, *J. Alloy. Compd.* 509 (2011) 596.
14. C. Hong, A. Noviyanto, J. H. Ryu, J. Kim, D. Yoon, *Ceram. Int.* 38 (2012) 301
15. Y.R. Zhu, L.C. Yin, T.F. Yi, H.P. Liu, Y. Xie, R.S. Zhu, *J. Alloy. Compd.* 547 (2013) 107.
16. J.J. Huang, Z.Y. Jiang, *Electrochim. Acta* 53 (2008)7756.
17. N.Q. Zhang, Z.M. Liu, T.Y. Yang, C.L. Liao, Z.J. Wang, K.N. Sun, *Electrochem. Commun.* 13 (2011) 654.
18. T. Yuan, K. Wang, R. Cai, R. Ran, Z.P. Shao, *J. Alloy. Compd.* 477 (2009) 665.
19. T. Yuan, R. Cai, K. Wang, R. Ran, S.M. Liu, Z.P. Shao, *Ceram. Int.* 35 (2009) 1757.
20. H.G. Jung, J. Kim, B. Scrosati, Y.K. Sun, *J. Power Sources* 196 (2011) 7763.
21. F.X. Wu, Z.X. Wang, X.H. Li, H.J. Guo, P. Yue, X.H. Xiong, Z.J. He, Q. Zhang, *Electrochim. Acta* 78 (2012) 331.
22. J.J. Huang, Z.Y. Jiang, *Electrochem. Solid-State Lett.* 11 (2008) A116.
23. G.Y. Liu, H.Y. Wang, G.Q. Liu, Z.Z. Yang, B. Jin, Q.C. Jiang, *J. Power Sources* 220 (2012) 84.
24. X. Li, C. Lai, C.W. Xiao, X.P. Gao, *Electrochim. Acta* 56 (2011) 9152.
25. X.F. Guo, C.Y. Wang, M.M. Chen, *Mater. Lett.* 83 (2012) 39.
26. W. Wang, J.G. Tu, S.B. Wang, J.G. Hou, H.M. Zhu, S.Q. Jiao, *Electrochim. Acta* 68 (2012) 254.
27. B.K. Guo, Y. Li, Y.F. Yao, Z. Lin, L.W. Ji, G.J. Xu, Y.Z. Liang, Q. Shi, X.W. Zhang, *Solid State Ionics* 204-205 (2011) 61.
28. Y. Qiao, X.L. Hu, Y. Liu, Y.H. Huang, *Electrochim. Acta* 63 (2012) 118.
29. X. Cao, C. Yuan, X. Tang, L. Xie, X. Liu, H. Wang, X. Yan, *J. Iran. Chem. Soc.* 6 (2009) 698.
30. X.Y. Cao, L.X. Zhang, B. Yang, X. Liu, D.W. Song, L.B. Qu, *Int. J. Electrochem. Sci.* 6 (2011)

4239.

31. L.L. Xie, L.Q. You, X.Y. Cao, C.F. Zhang, D.W. Song, L.B. Qu, *Electron. Mater. Lett.* 8 (2012) 411.
32. Y.Q. Wang, L. Guo, Y.G. Guo, L. Hong, X.Q. He, S. Tsukimoto, Y. Ikuhara, L.J. Wan, *J. Am. Chem. Soc.* 134 (2012) 7874.
33. G. Du, N. Sharma, V. K. Peterson, J. A. Kimpton, D. Jia, Z. Guo, *Adv. Funct. Mater.* 21 (2011) 3990.
34. G.Y. Liu, H.Y. Wang, G.Q. Liu, Z.Z. Yang, B. Jin, Q.C. Jiang, *Electrochim. Acta* 87 (2013) 218.
35. C.S. Cha, *Introduction to Kinetics of Electrode Process, third edition*, Science Press, Beijing (2002).
36. A.J. Bard, L.R. Faulkner, *Electrochemical Methods, second edition*, Wiley, New York (2001).
37. Y.H. Rho, K. Kanamura, *J. Solid State Chem.* 177 (2004) 2094.